JCB Journal of Cell Biology

ARTICLE

Retargeting of macroH2A following mitosis to cytogenetic-scale heterochromatic domains

Hanae Sato[1,2], Bin Wu[2,3], Fabien Delahaye[1,4], Robert H. Singer[2,3,5,6], and John M. Greally[1]

The heritability of chromatin states through cell division is a potential contributor to the epigenetic maintenance of cellular memory of prior states. The macroH2A histone variant has properties of a regulator of epigenetic cell memory, including roles controlling gene silencing and cell differentiation. Its mechanisms of regional genomic targeting and maintenance through cell division are unknown. Here, we combined in vivo imaging with biochemical and genomic approaches to show that human macroH2A is incorporated into chromatin in the G1 phase of the cell cycle following DNA replication. The newly incorporated macroH2A retargets the same large heterochromatic domains where macroH2A was already enriched in the previous cell cycle. It remains heterotypic, targeting individual nucleosomes that do not already contain a macroH2A molecule. The pattern observed resembles that of a new deposition of centromeric histone variants during the cell cycle, indicating mechanistic similarities for macrodomain-scale regulation of epigenetic properties of the cell.

Introduction

Epigenetic properties of cells are those involving differentiation decisions and memories of past events (Lappalainen and Greally, 2017). These properties are believed to be mediated at the molecular level by a number of transcriptional regulatory mechanisms. A necessary property of these epigenetic regulators of transcription is that they remain targeted to the same genomic regions in daughter chromatids following cell division and only change with cellular differentiation. The replication of DNA introduces unmodified nucleotides, creating daughter chromatids with hemimethylation of cytosine, the presence of 5-methylcytosine (5mC) on the template strand, but not the complementary, newly synthesized strand. This transient, hemimethylated state is recognized and targeted for enzymatic reestablishment of 5mC on both strands (Bostick et al., 2007; Sharif et al., 2007). DNA replication also disrupts the association of proteins with DNA as the replication fork passes through a region, using preexisting histones as well as freshly synthesized histones that lack the posttranslational modifications (PTMs) of the parent nucleosome to form new nucleosomes (Xu et al., 2010). While DNA methylation has a well-described biochemical mechanism for heritability through cell division, it has been more difficult to demonstrate comparable mechanisms for self-propagating maintenance of chromatin states. The symmetrical inheritance of core histones in daughter chromatids appears to be under active regulation by the MCM2 helicase in mammalian cells (Petryk et al., 2018), whereas in yeast, this symmetry is dependent on the leading-strand DNA polymerase, Pol ε (Yu et al., 2018). Posttranslationally modified histones become part of the daughter chromatids and appear to be capable of self-propagation, exemplified by the histone H3 lysine 27 trimethylation (H3K27me3) modification persisting in generations of daughter cells over multiple cell divisions, even when the polycomb repressive complex 2 (PRC2), which catalyzes this PTM, is inactivated in *Caenorhabditis elegans* (Gaydos et al., 2014) and in *Drosophila melanogaster* (Coleman and Struhl, 2017). Comparable findings have been revealed using nascent chromatin capture and amino acid isotope-labeling experiments (Alabert et al., 2015). Recent studies have revealed the kinetics of reconstitution of chromatin organization during mitosis (Reverón-Gómez et al., 2018), including the observation that activating marks tend to be lost but repressive marks are retained locally during chromatin reassembly (Ginno et al., 2018). As we have previously noted (Henikoff and Greally, 2016), a model for the self-propagation of H3K27me3 is based on the ability of PRC2 to bind specifically to this modification (Hansen et al., 2008), suggesting that this binding tethers the PRC2 complex so that it

[1]Center for Epigenomics and Department of Genetics, Albert Einstein College of Medicine, Bronx, NY; [2]Department of Anatomy and Structural Biology, Albert Einstein College of Medicine, Bronx, NY; [3]Gruss Lipper Biophotonics Center, Albert Einstein College of Medicine, Bronx, NY; [4]Department of Obstetrics and Gynecology and Women's Health, Albert Einstein College of Medicine, Bronx, NY; [5]Dominick P. Purpura Department of Neuroscience, Albert Einstein College of Medicine, Bronx, NY; [6]Janelia Research Campus, Howard Hughes Medical Institute, Ashburn, VA.

Correspondence to John M. Greally: john.greally@einstein.yu.edu; Robert H. Singer: robert.singer@einstein.yu.edu; B. Wu's present address is Department of Biophysics and Biophysical Chemistry, Johns Hopkins University School of Medicine, Baltimore, MD.

can then add H3K27me3 onto other nearby nucleosomes after replication. How these chromatin states are initially targeted to specific regions is also a focus of investigation. The targeting of H3K27me3 in *D. melanogaster* appears to require the presence of polycomb-response elements (Laprell et al., 2017), which mediate sequence-specific targeting by binding transcription factors, which then recruit the PRC2 complex. The mechanism of initial targeting in mammalian cells remains less well understood.

There are other reasons why chromatin states can be the same in parent and daughter cells. These include chromatin states that are established as secondary consequences of other genomic processes. The passage of RNA polymerase through a region while transcribing a gene is associated with the local enrichment of PTMs such as H3K36me3, mediated by direct interaction of the Set2 lysine methyltransferase with RNA polymerase (Kizer et al., 2005). Histone PTMs at short regulatory elements flanking nucleosome-free regions are plausibly mediated by the recruitment of enzymatic complexes by transcription factors (Henikoff and Greally, 2016), while short RNAs such as the piwi-interacting RNAs have been found to direct local repressive chromatin states at transposable elements in *D. melanogaster* (Le Thomas et al., 2013). More difficult to understand mechanistically has been the formation and maintenance through cell division of large chromatin domains exceeding tens of kilobases. Domains of this magnitude include the mediators of certain long-term cellular memories, such as the inactivation of an X chromosome during dosage compensation at the blastocyst stage of mammalian development (Augui et al., 2011) or the imprinting of large genomic domains during gametogenesis (Ferguson-Smith, 2011). Some of these larger-scale chromatin states involve the deposition of histone variants into nucleosomes in those regions. Histone variant deposition can be very focal, such as histone H3.3, which is enriched at cis-regulatory sites and telomeres (Goldberg et al., 2010), but others are maintained in broad genomic regions, such as CENP-A at centromeric chromatin, occupying regions up to several million contiguous base pairs in size (Cleveland et al., 2003) and propagating to daughter chromatids through processes that are increasingly well understood (reviewed in Müller and Almouzni, 2014). The histone variant macroH2A also forms broad chromatin domains of at least hundreds of kilobases (Gamble et al., 2010) but is not limited to a discrete chromosomal location like the centromere, instead distributing genome-wide. MacroH2A differs from canonical H2A by having an additional C-terminal, ∼25-kD globular domain (Pehrson and Fried, 1992) and has been shown to have roles both in the maintenance of cell states and in cell fate decisions (Creppe et al., 2012; Pasque et al., 2012; Barrero et al., 2013). The presence of macroH2A locally in the genome is mostly associated with transcriptional silencing, with striking enrichment at the inactive X chromosome territory in mammalian cells (Costanzi and Pehrson, 1998; Chadwick and Willard, 2002). Unlike other histone variants (Gurard-Levin et al., 2014), chaperones that target macroH2A to chromatin have not yet been identified, except in the specific situation of DNA damage, which involves macroH2A interacting with the Aprataxin-PNK–like factor (Mehrotra et al., 2011). The loss of ATRX in the cell has been associated with a more permissive distribution of macroH2A into the α globin domain (Ratnakumar et al., 2012), suggesting that ATRX normally prevents the association of macroH2A with chromatin in this genomic region. Therefore, while we can implicate macroH2A as a potential contributor to the epigenetic property of cellular memory involved in X inactivation, we lack insight into how macroH2A propagates its genomic organization faithfully from parent to daughter cells, targeting specific regions of the genome, prompting the current study.

Results

To gain insights into how macroH2A remains targeted to specific genomic contexts through mitotic cell division, we performed a combination of imaging, biochemical, and genomic techniques. We established the SNAP labeling system (Gautier et al., 2008) for macroH2A1.2 in HEK 293T cells. As HEK 293T cells have three X chromosomes, of which two are inactivated, the labeled macroH2A generates two strong X chromosome territory signals in each nucleus, a valuable marker of the stability and homogeneity of the modified cell line (Fig. S1). We used SNAP labeling combined with cell synchronization to demonstrate that we could distinguish macroH2A incorporated during the prior cell cycle from newly incorporated macroH2A in the subsequent cell cycle using separate fluorophores (Fig. S2 A). HEK 293T cells in prometaphase were collected following 12 h of nocodazole blocking by mitotic shake-off, labeling the macroH2A present from the preceding cell cycle with SNAP–Oregon Green. The cells were then released from arrest at the G2/M transition, pulsed with SNAP-block to prevent any unconjugated macroH2A from detection by fluorophores, and returned to cell culture, arresting the cells at the next G2/M transition using RO-3306. Newly incorporated macroH2A was detected with a distinctive red fluorophore using SNAP-TMR Star. This allowed live-cell imaging during mitosis to be performed, measuring the levels of Oregon Green and TMR-Star in the dividing cells every 15 min (Fig. S2 B and Video 1). The result showed that preexisting macroH2A remained associated with chromatin following mitosis and that both preexisting and newly incorporated macroH2A were evenly distributed into each of the daughter cells (Fig. S2 C).

We then tested the timing of incorporation of macroH2A. First, we determined incorporation timing of endogenous macroH2A1 through cell cycle by Western blot. Cells were harvested before and after S phase, and Western blot showed the expected increases in replication-dependent incorporation of histone H3 (Xu et al., 2010) and mitosis-associated enrichment of histone H3 serine 10 phosphorylation (Van Hooser et al., 1998) but little change in macroH2A1 (Fig. 1 A). We then applied an imaging-based approach to address the same question using the cell-synchronization and SNAP-labeling approach shown in Fig. 1 B. We also added labeling with 5-ethynyl-2′-deoxyuridine (EdU) as a further means of confirmation that cells were in the S phase of the cell cycle. We quantified the ratio of red (new) to green (old) histone in each cell for SNAP-H3 and SNAP-macroH2A (examples shown in Fig. 1 C). We demonstrated that the cells incorporated significantly more SNAP-H3 during

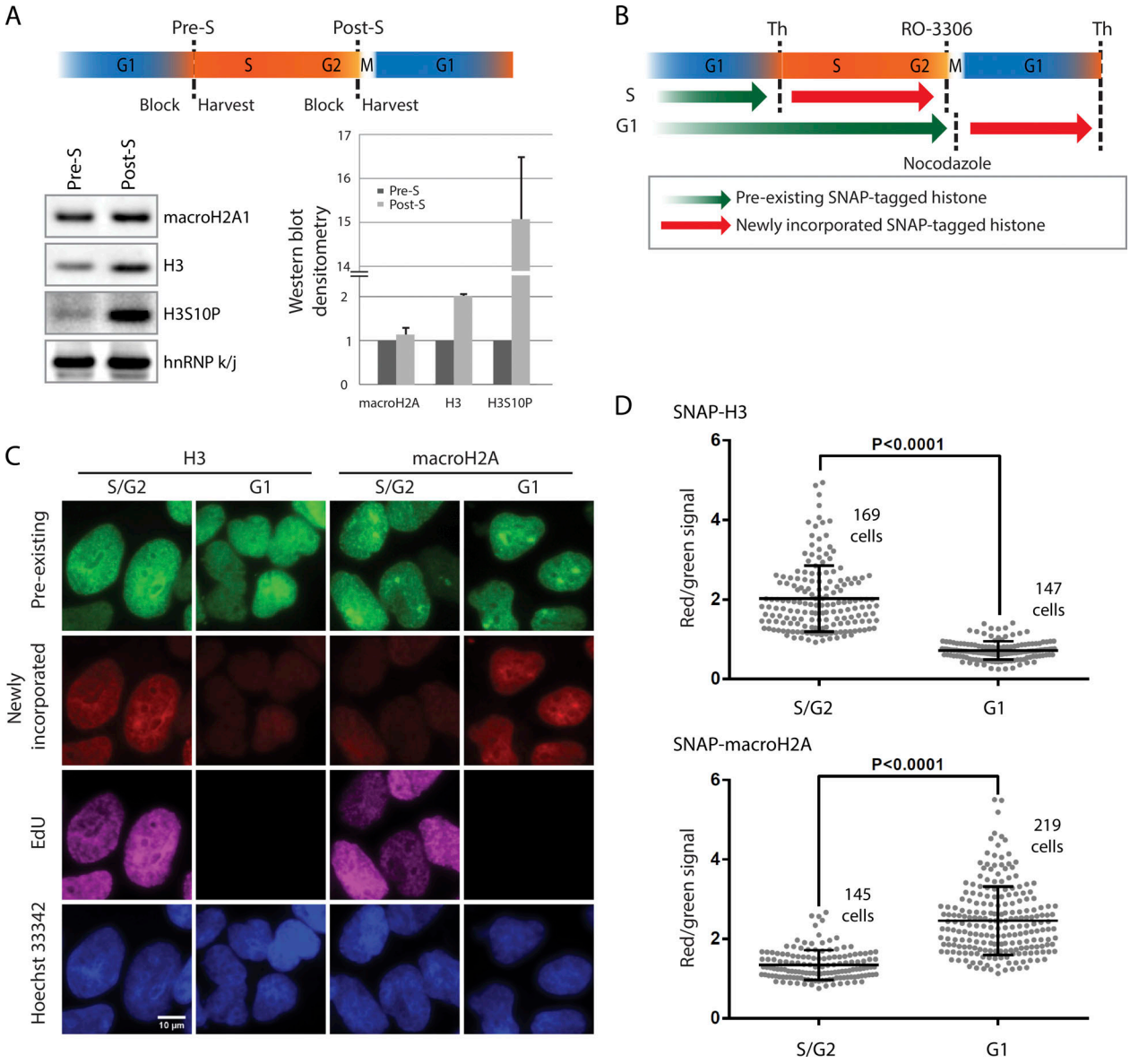

Figure 1. **Quantification of SNAP-macroH2A in S/G2 and G1 phases of the cell cycle. (A)** Western blot analysis of endogenous histone H3 and macroH2A before and after S phase. The time line of synchronization and harvesting of HEK 293T cells is shown. Equal numbers of cells were synchronized at the G1/S phase border by a double thymidine block. The cells were harvested, pre-S, or released from thymidine block and synchronized before M phase with RO-3306 and harvested, post-S. Chromatin fractions were isolated for Western blotting, testing endogenous macroH2A1, histone H3, and phosphorylation of H3 at serine 10 (H3S10P) as a marker of mitosis, with hnRNP k/j as a loading control. We show that H3 increases during mitosis, as expected, but there is no concurrent increase in macroH2A. Error bars represent standard deviation from three independent experiments. **(B)** The time line of synchronization and labeling of cells at S/G2 and G1 phases for the analysis in C. To label newly incorporated histones in S/G2 phase, HEK 293T cells stably expressing SNAP-tagged H3 or macroH2A were synchronized at the G1/S phase border by double thymidine block. Cells were treated with SNAP–Oregon Green to label preexisting histones (green arrow), subsequently blocking nonlabeled proteins using the nonfluorescent SNAP-Block reagent. The cells were allowed to progress to the G2/M transition until they were blocked using RO-3306 (a CDK1/cyclin B1 and CDK1/cyclin A inhibitor), labeling newly incorporated SNAP-tagged histones with SNAP-TMR Star (red arrow). To label newly incorporated histones in G1 phase, mitotic cells were collected by shake-off following nocodazole treatment for 12 h and spread onto coverslips. After 2 h, cells were labeled with Oregon Green and treated with the blocking reagent. Cells were then allowed to progress to the G1/S transition, when they were synchronized by double thymidine block, then labeling newly incorporated SNAP-tagged histones with SNAP-TMR Star (red arrow). After being released from the first synchronization, the cells were also incubated with EdU until the second synchronization, allowing cells that had undergone DNA synthesis to be identified. **(C)** An example of images showing the detection of preexisting and newly synthesized SNAP-tagged histones in S/G2 or G1 phases. Bar = 10 µm. **(D)** Image analysis measurements of red and green nuclear signals, representing the ratio of newly incorporated to preexisting histones H3 and macroH2A in the S/G2 and in G1 phases. The error bars represent one standard deviation from the number of single cells that indicated on each dataset. The P values were determined using two-tailed unpaired *t* tests.

S/G2 compared with the G1 phase (Fig. 1 D), once again consistent with the property of histone H3 being incorporated into chromatin during replication (Xu et al., 2010). By contrast, SNAP-macroH2A showed a distinctive pattern of strong enrichment in G1, but not S/G2 (Fig. 1 D), indicating that its incorporation was not dependent on ongoing DNA replication.

While X chromosome inactivation can occur in the absence of macroH2A (Tanasijevic and Rasmussen, 2011), macroH2A1 appears to work synergistically with the PRC1 polycomb complex and the CULLIN3/SPOP ubiquitin E3 ligase to stabilize inactivation (Hernández-Muñoz et al., 2005), and it appears to be recruited by the *Xist* long noncoding RNA (Csankovszki et al., 1999). The inactive X is also notable for its late replication timing during S/G2 (Koren and McCarroll, 2014), raising the question whether there is a distinctive pattern of deposition of macroH2A during the cell cycle in the inactive X chromosome compared with the rest of the genome. We partitioned the nuclear signal into the subnuclear domains containing the two inactive X chromosomes and the remainder of the nucleus. The inactive X territories were apparent from the preexisting macroH2A signals. The relative signal from SNAP-macroH2A within these territories was compared with the remainder of the nucleus. We found the incorporation of macroH2A into the inactive X chromosomes occurred at the same time as the remainder of the genome, during the G1 phase of the cell cycle, and that it appeared to localize preferentially to the inactive X chromosome territories (Fig. 2).

We then performed a time course experiment to gain more precise insights into the timing of deposition of macroH2A during the cell cycle. Cells were synchronized at the G1/S transition using a double thymidine block and then released and cultured for up to 22 h (Fig. 3 A). Four fluorophores were used in these cells, two for SNAP labeling of macroH2A and two for the Fucci cell cycle sensor system (Sakaue-Sawano et al., 2008). The cells were then sampled every 2 h and tested using flow cytometry to quantify the intensities of signals of preexisting SNAP-macroH2A (green) and newly incorporated macroH2A (red). We show in Fig. 3 B that the intensity per cell of preexisting SNAP-macroH2A drops suddenly at 12 h. Parallel studies using the Fucci cell cycle sensor system shows the HEK 293T cells to be in S/G2 until 10 h with a change to G1 at 12 h (Fig. S3). The decrease of signal intensity of preexisting macroH2A therefore coincides with cells undergoing mitotic division and the dilution of the preexisting macroH2A into two daughter cells. The signal for newly incorporated SNAP-macroH2A, on the other hand, began to be observed at 18 h, during the G1 phase.

We complemented these flow cytometry studies with live-cell imaging to gain more detailed resolution of the timing of acquisition of newly incorporated SNAP-macroH2A. Representative results are shown in Fig. 4 A (and Videos 2 and 3), with the summary of the imaging of 22 cells in Fig. 4 B. We measured the signal intensity of newly incorporated macroH2A, normalized by the signal from preexisting macroH2A, and calibrated for each cell the stage of the cell cycle using the Fucci signals. We found that the single period of consistent macroH2A incorporation was between hours 13 and 17 (red box), starting immediately after metaphase and extending to mid-G1 phase (Fig. 4 B).

Knowing that new macroH2A was being incorporated during early G1, we could then ask whether it was being targeted at that time to the genomic regions where the macroH2A had been incorporated in the parent cell. We again exploited the SNAP labeling system to conjugate biotin to preexisting and newly incorporated macroH2A, as shown in Fig. 5 A. We performed the equivalent of native chromatin immunoprecipitation (ChIP) using SNAP-biotin instead of antibodies to enrich the subset of nucleosomes with SNAP-macroH2A. We refer to this technique as affinity chromatin enrichment (AChE) and show the principle of the assay in Fig. 5 B. We recover the mononucleosomes containing SNAP-macroH2A to which SNAP blocker is not conjugated. In the nocodazole-treated cells (Fig. 5 A, lower condition), the SNAP-macroH2A being actively incorporated during G1 will be present in a subset of nucleosomes and can be conjugated to the biotin for enrichment using streptavidin beads. In the RO-3306–treated cells (Fig. 5 A, upper condition), mononucleosomes containing SNAP-macroH2A are unlikely to have been incorporated in S–G2, based on the data shown in Figs. 1, 2, 3, and 4, and are more likely to represent those incorporated in G1 of the previous cell cycle and incompletely blocked. The S/G2 and G1 libraries were sequenced in parallel with an input sample on which the same affinity protocol was performed but without conjugating biotin to the SNAP tag.

Previous studies mapping the locations of macroH2A in mammalian cells revealed it to be enriched in very broad domains, requiring modification of standard ChIP sequencing (ChIP-seq) peak calling approaches (Gamble et al., 2010; Yildirim et al., 2014). We therefore started our AChE analysis by testing the enrichment patterns in genomic windows of different sizes (Fig. S4 A). The expected pattern is of enrichment in some genomic locations relative to others, resulting in a bimodal distribution of sequencing reads from those loci when comparing affinity-purified against input mononucleosomal samples. Using windows of 1–1,000 kb, we observed the transition to a bimodal distribution indicating enrichment only at and above 500-kb resolution. We defined the inflection point separating the loci of macroH2A enrichment for the S/G2 and G1 phases of the cell cycle using the *pastecs* R package (Fig. S4 B). The enriched 500-kb windows identified in this way represented our highest confidence loci for macroH2A deposition in the genome, allowing us to test how concordant these loci were during G1 and S/G2 phases of cell cycle. The degree of enrichment in Fig. S4 B is less than would be expected for point source chromatin states occurring in only a small proportion of the genome but is typical for those that exist broad domains (Bailey et al., 2013). Of the 831 windows with macroH2A enrichment during S/G2 phase, 810 (97.6% of windows in S/G2 phase) remained enriched in G1 phase at loci of newly incorporated macroH2A (Fig. 5 C). Visual inspection of the results indicated that the windows of enrichment were located especially in Giemsa dark (G-) bands (Fig. S4), which we confirmed through permutation studies of randomly redistributed windows of enrichment of macroH2A and UCSC Genome Browser annotations of cytogenetic bands (Figs. 5 D and S4). We tested the enrichment per megabase for each chromosome and added a calculation that assumed enrichment for macroH2A on only the two of the three X chromosomes that

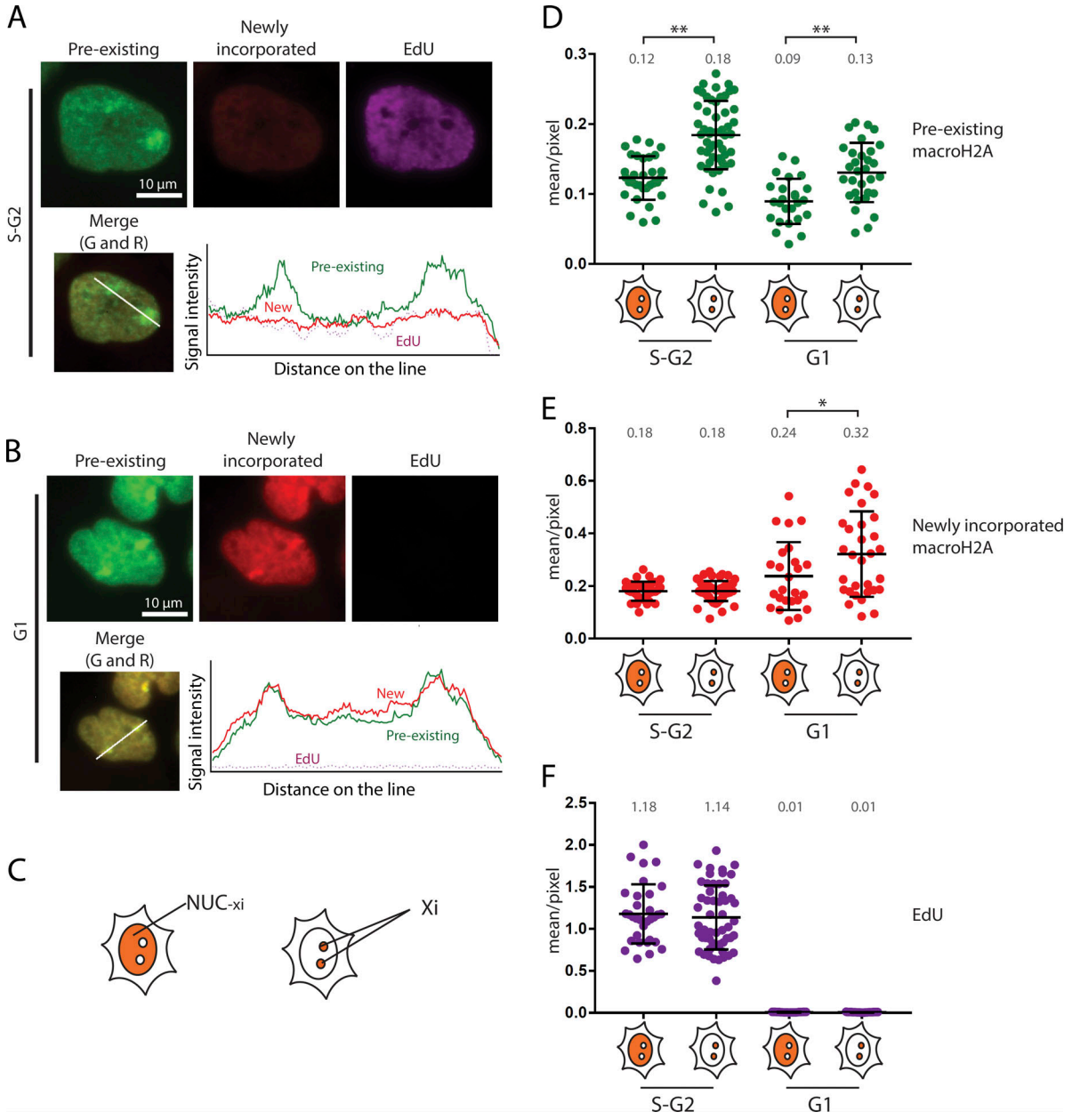

Figure 2. **Pulse-chase detection of macroH2A incorporation into the inactive X chromosome territory.** HEK 293T cells stably expressing SNAP-tagged macroH2A were synchronized and pulse-chase labeled as shown in Fig. 1 B. **(A)** Image analysis of SNAP-tagged macroH2A incorporation on the two inactive X chromosomes (Xi) in HEK 293T cells during S-G2 phase. The top images show (from left) the images of preexisting (Oregon Green, green), newly incorporated (TMR, red) SNAP-macroH2A, and EdU labeling. The lower left image shows the merged images of preexisting and newly incorporated SNAP-macroH2A. In the lower right panel, we show the signal intensities measured along the white dashed lines in the images of preexisting and newly incorporated (TMR, red) SNAP-macroH2A, and EdU labeling. The green, red, and magenta lines show the signal intensities of preexisting and newly incorporated macroH2A and EdU, per pixel, respectively. The levels of intensities were obtained using Color Profiler in ImageJ. **(B)** The same types of images as in A but during G1 phase. **(C)** We illustrate the areas measured. NUC_{-Xi} is the entire area of the nucleus excluding the two inactive X chromosomes (Xi). **(D)** The signal intensities of preexisting macroH2A in NUC_{-xi} and Xi, showing the increased signal in the Xi territories in both S-G2 and G1. **(E)** A comparison of the signal intensities of newly incorporated macroH2A between the NUC_{-Xi} and Xi subnuclear domains in S/G2 and in G1. With the minimal signal in S–G2, no enrichment of the Xi territories occurs, but significant enrichment is found in G1. **(F)** The signal intensities of EdU incorporation in the NUC_{-Xi} and Xi domains. In D and E, each intensity per pixel was normalized by Hoechst intensity to take into account local chromatin compaction. In D–F, the number above the data points indicates the mean value, P values were determined using unpaired *t* tests (*, $P < 0.04$; **, $P < 0.001$). Error bars represent standard deviation from the number of single cells that indicated on each dataset in Fig. 1 D. We conclude that the inactive X chromosome is preferentially targeted for macroH2A deposition compared with the rest of the nucleus.

are inactivated, which supports a preferential deposition of macroH2A on the X chromosomes (Fig. S4 C) consistent with our imaging studies. Using quantitative PCR (qPCR), we showed that the loci in windows with predicted macroH2A deposition were indeed enriched (Fig. 5 E). These genomic localization studies therefore showed macroH2A to be enriched in very large

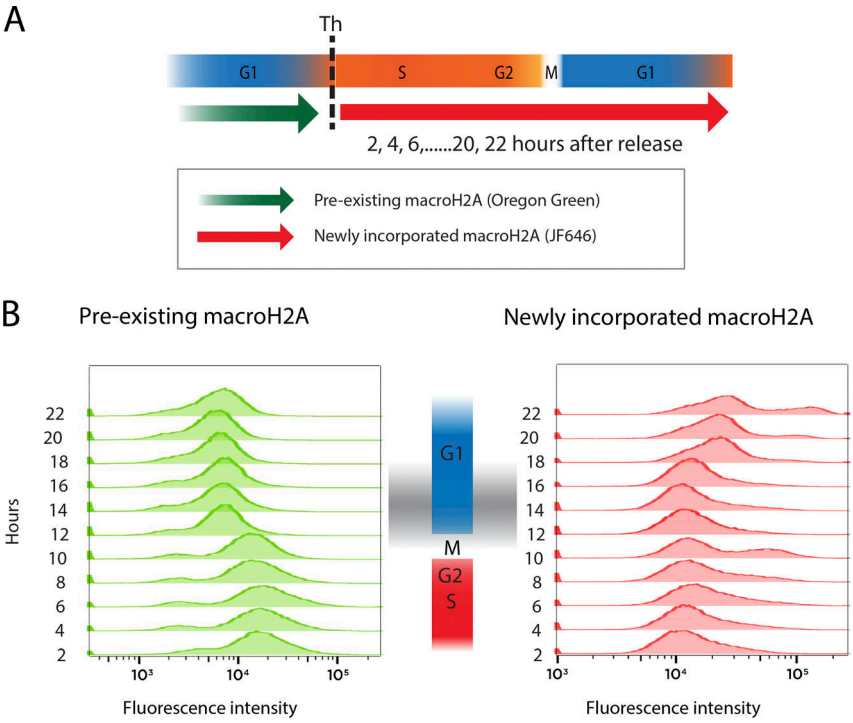

Figure 3. **Flow cytometric timing of SNAP-macroH2A incorporation. (A)** The time line of synchronizing and labeling cells. Newly synthesized macroH2A was labeled with SNAP substrate JF646 at each 2-h time point after release from thymidine block. **(B)** Flow cytometric analysis of preexisting (Oregon Green) and newly incorporated macroH2A (JF646), with cell cycle timing data derived from Fucci experiments shown in Fig. S3. The gray shading illustrates the interval of transition from preexisting macroH2A (hours 2–10, S/G2) to an enrichment for newly incorporated macroH2A (hours 18–22, G1).

domains of hundreds of kilobases, especially in the cytogenetic G-bands representing constitutive heterochromatin, and that newly incorporated macroH2A in G1 targets the loci already enriched for macroH2A in the parent cell. While not a focus of their report, published immunofluorescence images of macroH2A show banding patterns (Chadwick and Willard, 2002), suggesting that the domains of macroH2A identified by AChE-seq may be cytogenetically apparent.

The question that arose was how macroH2A recognizes these heterochromatic regions already enriched for this histone variant. In eukaryotic cells, the chromatin is organized by the basic unit of the nucleosome, which is composed by two dimers of H2A-H2B and a tetramer of H3-H4 in 147 bp of DNA. We tested the simplest possible model that macroH2A recognizes individual nucleosomes that already contain both macroH2A and H2A heterotypically and replaces the existing H2A with a second macroH2A molecule to create a homotypic nucleosome. We prepared mononucleosomes (Fig. 6 A) and used an anti-SNAP antibody to isolate the subset of nucleosomes containing a SNAP-macroH2A (Fig. 6 B). Using an anti-macroH2A1 antibody and Western blotting, we tested whether these nucleosomes also included endogenous macroH2A, which would indicate the presence of nucleosomes homotypic for macroH2A. The HEK 293T cell line used for all assays in this project (except where indicated otherwise) was chosen for low expression levels of SNAP-macroH2A (30% of endogenous macroH2A; Fig. S5 A) to reduce the chance of perturbing endogenous macroH2A expression, as has been found previously in transgenic cell lines (Borghesan et al., 2016). Even using the low-expressing SNAP-macroH2A cell line, endogenous macroH2A could not be detected in the nucleosomes containing SNAP-macroH2A (Fig. 6 B).

We then applied fluorescence correlation spectroscopy (FCS; Chen and Müller, 2007) to test this question in an orthogonal manner. FCS allows the quantification of fluorescence intensity of single molecules in solution, in this case allowing us to test whether the single nucleosomes isolated contained more than one SNAP-tagged molecule, indicating a homotypic organization of the histone variant. For these experiments, we switched to a cell line expressing SNAP-macroH2A at a high level (threefold higher than endogenous macroH2A1; Fig. S5 A), increasing the chance of finding nucleosomes with two SNAP-macroH2A molecules in any homotypic nucleosomes present. To ensure that we were saturating the labeling of SNAP-macroH2A, so that any subset of nucleosomes containing two SNAP-macroH2A molecules would reliably show two fluorescent molecules, we defined and used the saturating conditions for SNAP labeling (Fig. S5 B). We measured the fluorescence intensity per unit volume of a solution containing single nucleosomes saturated for SNAP-macroH2A labeling compared with a solution containing individual SNAP–Oregon Green molecules. In Fig. 6 C, we show that the signal intensity per nucleosome is indistinguishable from that of single SNAP–Oregon Green molecules, demonstrating that only single SNAP-tagged macroH2A molecules are detected in individual nucleosomes. Our results are consistent with the prediction that macroH2A is likely to be unstable when present homotypically in a nucleosome (Chakravarthy and Luger, 2006) and exclude the possibility of incorporation of new macroH2A into nucleosomes already containing macroH2A as the mechanism of targeting macroH2A during G1 phase to genomic regions already enriched in this histone variant.

Finally, we estimated the approximate proportion of nucleosomes in the human genome containing a macroH2A molecule. We used cell lines expressing either SNAP-macroH2A or SNAP-H3 and isolated mononucleosome preparations that were loaded onto a Western blot (Fig. S5 C). Detection with an anti-H3

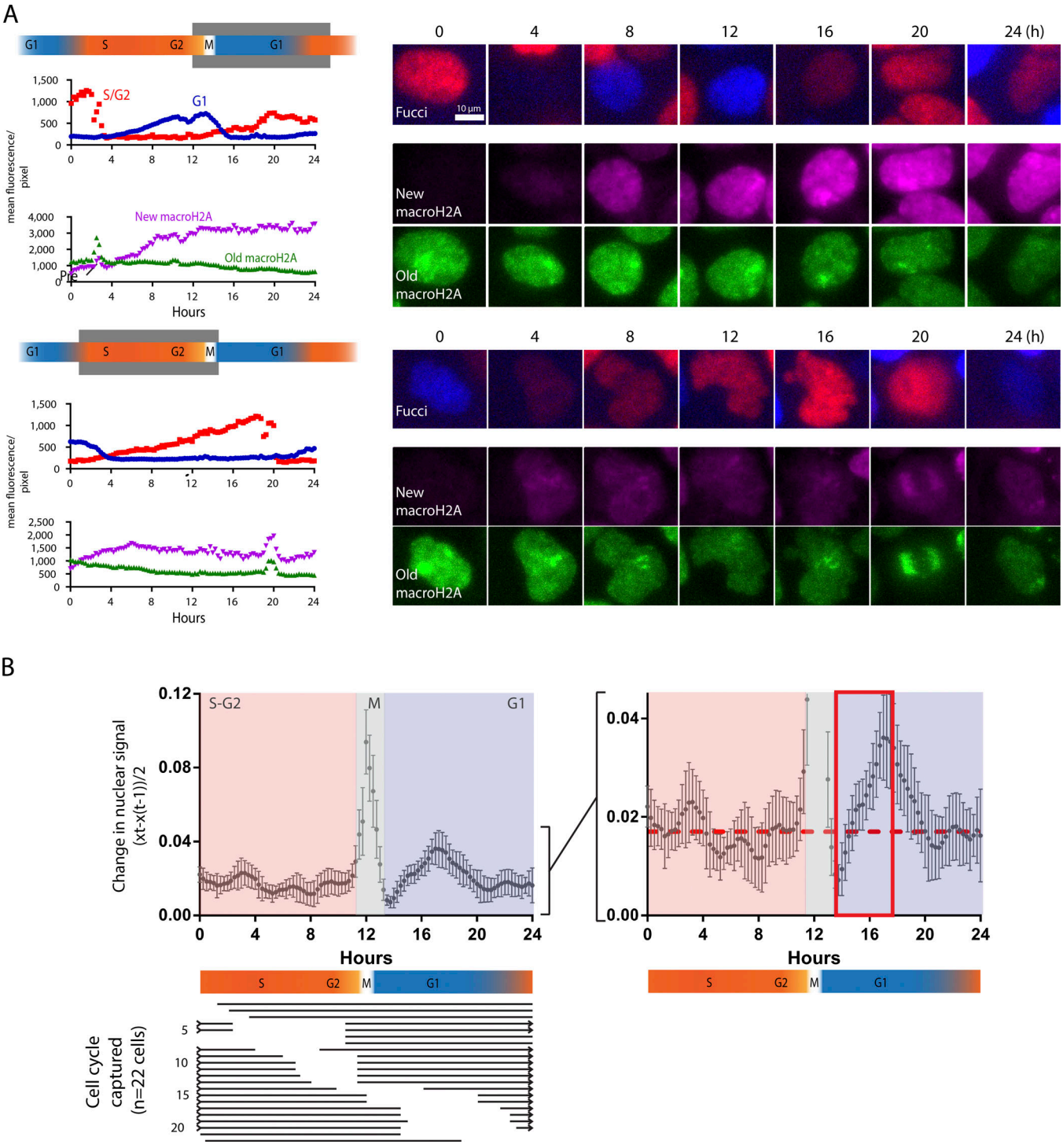

Figure 4. **Real-time in vivo imaging of SNAP-macroH2A incorporation timing. (A)** Examples of in vivo imaging of macroH2A dynamics in individual cells. Preexisting macroH2A in nonsynchronized cells was labeled with SNAP–Oregon Green and blocked with SNAP-Block. Newly incorporated macroH2A was detected with JF646. Live-cell images were acquired every 20 min for 18–20 h. Signal intensity transitions were measured as shown in the left panels (Fucci, upper: S/G2, red; G1, blue; SNAP-tagging; lower: preexisting macroH2A, green; newly incorporated macroH2A, magenta). Representative images from four hourly intervals are shown to the right (with the component of the cell cycle captured shown with a gray box). The upper cell is captured entering G1 and shows a substantial accumulation of new macroH2A, whereas the lower cell is captured during S/G2 and accumulates new macroH2A to a much lesser extent. **(B)** The summarized data from imaging of 22 cells. The cells were aligned temporally using the Fucci cell cycle images. The lines in lower panel represent the detection phase in each cell. The rate of change of signal of newly incorporated macroH2A was calculated as the difference of intensity of newly incorporated macroH2A normalized to the signal in first time point of preexisting macroH2A between two consecutive time points [Delta $(X_t - X_{(t-1)})/2$]. These delta values were then plotted through the cell cycle. Signal saturation at metaphase distorts the data, but the right panel allows comparison of temporal changes compared with the average delta (0.17) during S–G2 phase. The period of sustained accumulation of macroH2A is between hours ∼13 and 17 (red box). Error bars represent standard error of the mean from 22 cells.

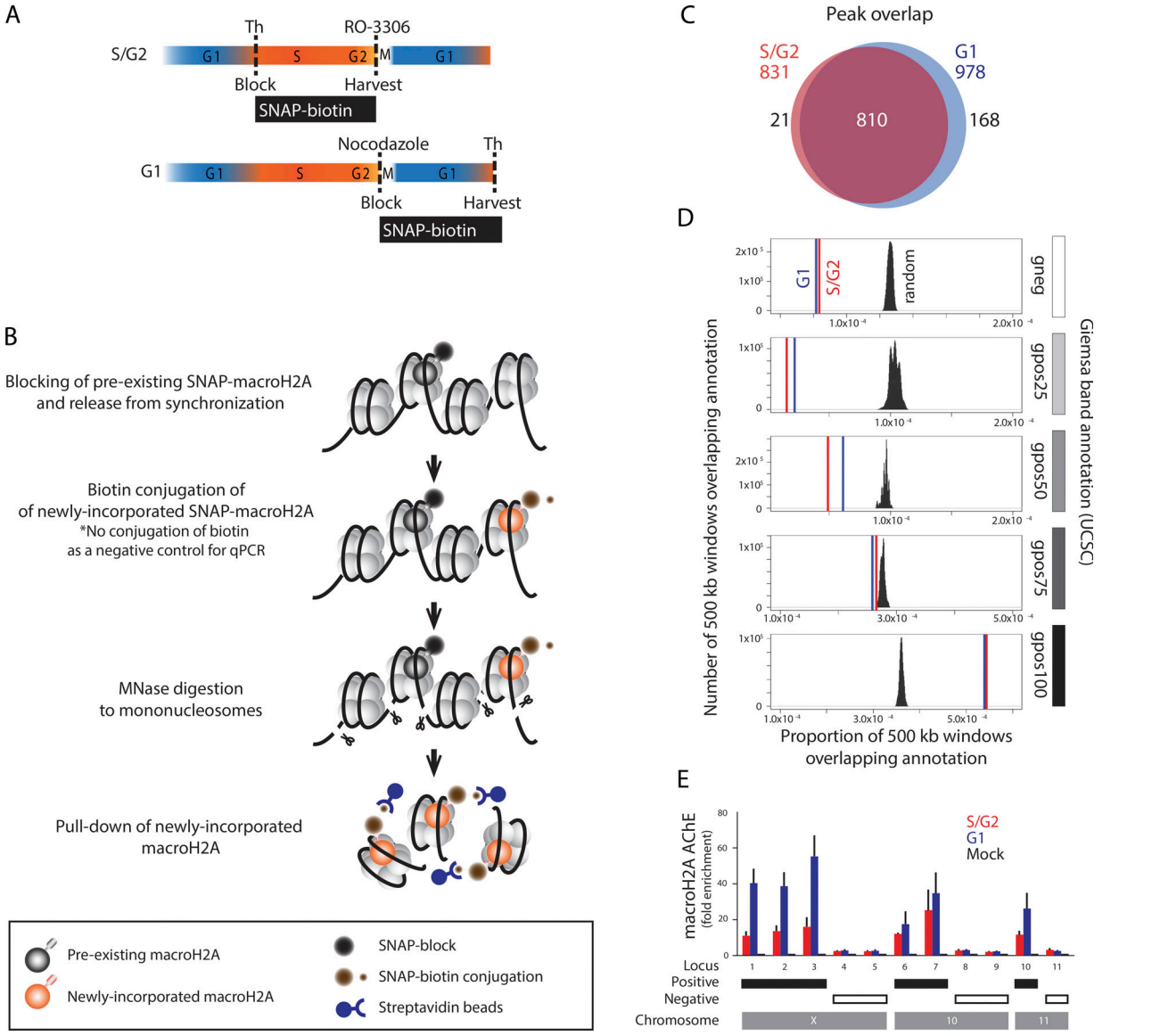

Figure 5. **Cell cycle–specific AChE-seq studies of macroH2A incorporation in S/G2 and G1 phases of the cell cycle. (A)** The time line of synchronizing, blocking, and harvesting of cells. **(B)** The experimental overview of AChE. **(C)** MacroH2A enrichment "peaks" overlap substantially between macroH2A newly incorporated in S/G2 and in G1. **(D)** MacroH2A is enriched before and after cell division in Giemsa-positive bands, specifically those categorized as gpos100 in the UC Santa Cruz Genome Browser. The results of permutation tests demonstrate enrichment only for the most heterochromatic cytogenetic bands ($P < 0.01$). **(E)** AChE-qPCR of loci predicted from the AChE-seq results to be positive and negative validates these genome-wide studies. Pull-down without SNAP-biotin treatment was used as negative controls (mock). The graph shows means and standard deviations from three independent experiments.

antibody allowed a loading control for mononucleosome numbers, showing the endogenous and SNAP-tagged H3 proteins. Using the same Western blot, detection with an anti-SNAP antibody revealed the difference in expression levels of the transgenes, while detection with anti-macroH2A showed us the relative expression levels of the transgenic and endogenous macroH2A genes. This in turn allowed us to estimate the proportion of nucleosomes in the SNAP-H3 cell line containing macroH2A, calculated as 24.2%. Genome-wide, it therefore appears that approximately one nucleosome in every four contains a macroH2A histone variant, probably occurring at much higher proportions in G-bands and lower proportions in the remaining majority of the genome.

Discussion

The combination of approaches used in this study has revealed insights into the heritability through cell division of a chromatin state that is organized over a scale of hundreds of kilobase pairs in the human genome. MacroH2A appears to occupy nucleosomes heterotypically with histone H2A, enriched in Giemsa dark G-bands, which are the most heterochromatic and late-replicating regions of the genome (Suzuki et al., 2011). These late-replicating regions in the genome are those targeted for deposition of new macroH2A in the hours following mitosis and cytokinesis, during the G1 phase in daughter cells. The mechanism for retargeting of macroH2A to these regions is unknown but does not involve recognition of and incorporation of

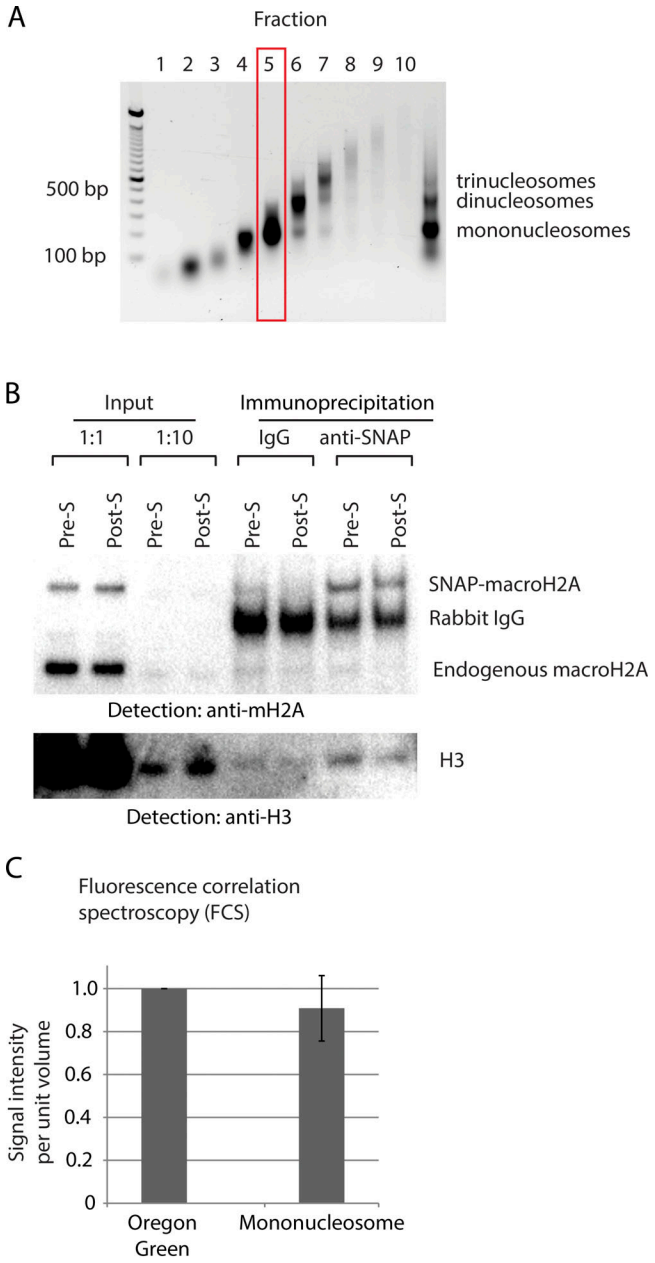

Figure 6. **Nucleosomal organization of macroH2A. (A)** Mononucleosomes (red box) were purified using high-density sucrose gradient ultracentrifugation of samples synchronized as in Fig. 1 A. **(B)** Western blotting before and after immunoprecipitation of pure mononucleosomes using anti-SNAP antibody or rabbit IgG as a negative control. Input samples (and 1:10 dilutions) were loaded in the four lanes on the left. The lower Western blot shows that histone H3 is present in the isolated mononucleosomes and that the loading of the pairs of samples before (pre-S) or after S phase (post-S) lanes is balanced. In the upper blot, there is no evidence for nucleosomes containing SNAP-macroH2A also containing detectable levels of endogenous macroH2A, as the signal intensities in the anti-SNAP lanes do not exceed those of the nonspecific IgG lanes. **(C)** The brightness of individual nucleosomes containing Oregon Green–labeled SNAP-macroH2A measured by FCS was indistinguishable from individual beads with single molecules of SNAP–Oregon Green, demonstrating that individual nucleosomes contain only single molecules of SNAP-macroH2A. The graph shows means and standard deviations from three independent experiments.

macroH2A into individual nucleosomes already containing macroH2A. As H2A is already present in the nucleosomes formed during daughter chromatid formation in S/G2, the subsequent targeting of macroH2A involves replacement of one of the two H2A molecules in individual nucleosomes.

This timing of incorporation of the macroH2A histone variant into chromatin following cell division in the G1 phase reveals a parallel with the physiology of the centromeric histone variant CENP-A (Jansen et al., 2007). CENP-A is the H3-like histone variant that is part of the specialized nucleosome forming the centromere (French and Straight, 2013). Human centromeres are estimated to be up to several million contiguous base pairs in size (Cleveland et al., 2003), a magnitude of the same order as that inferred from our AChE data for macroH2A. There is a strong preference in human cells to form centromeres at specific short satellite DNA sequences, but they can also be formed ectopically at other sequences and remain stable at those locations through cell division and across generations (Amor and Choo, 2002), representing a molecular mechanism for epigenetic maintenance of cellular memory. Following DNA synthesis and cell division, preexisting CENP-A remains at centromeres but is distributed between daughter chromatids with H3.3 (Dunleavy et al., 2011). The mechanism of the subsequent retargeting of these diluted locations with new CENP-A in G1 is not known, but may involve histone H3 lysine 4 dimethylation (H3K4me2) and the activity of the HJURP chaperone for CENP-A (Bergmann et al., 2011), which is in turn recruited to the mammalian centromere by the Mis18 complex (Wang et al., 2014) assisted by a centromeric long noncoding RNA (Quénet and Dalal, 2014). These observations about the centromere offer potential guidance into how we might study the targeting of macroH2A.

Another H2A variant, H2A.Z, is also incorporated into pericentric heterochromatin (PCH) in mammalian cells preferentially during the G1 phase of the cell cycle (Boyarchuk et al., 2014), which suggested to the authors a model of active eviction of preexisting histones at this stage of the cell cycle, prompted by their previous observations of H3.3 being evicted for CENP-A at centromeres during G1 (Dunleavy et al., 2011). Interestingly, the preexistence of a heterochromatic state in PCH influences how much H2A.Z is deposited in these regions but does not influence the timing of its incorporation (Boyarchuk et al., 2014). The example of X chromosome inactivation raises the question whether the long noncoding RNA *Xist* not only promotes the incorporation of macroH2A (Csankovszki et al., 1999) but also influences its timing of incorporation. However, as *Xist* is expressed throughout the cell cycle (Ng et al., 2011), this does not appear likely as the mechanism of timing of incorporation.

Our observation that macroH2A is preferentially targeted to cytogenetic bands with the characteristics of heterochromatin is consistent with its known property to maintain heterochromatic structures. When macroH2A was depleted in HepG2 cells, cytological changes in heterochromatin and nucleolar organization became apparent (Douet et al., 2017). The same study also found macroH2A to be associated with heterochromatic and H3K9me3-enriched regions of the genome, consistent with the findings presented here, and also demonstrated a role for macroH2A in the attachment of SAT2 repeats to Lamin B1 (Douet

et al., 2017). These authors concluded that macroH2A plays a significant role in maintaining nuclear architecture, in particular the association of heterochromatic, H3K9me3-enriched regions with the nuclear lamina, shedding light on one aspect of its functional role in the cell nucleus. At the nucleosomal level, how macroH2A exerts its repressive effects appears to involve the direct interference by the macroH2A tail domain of NF-κB binding to DNA locally and a resistance of chromatin containing macroH2A to SWI/SNF-mediated chromatin remodeling (Angelov et al., 2003). The repressive effects of macroH2A are therefore likely to be acting both at the level of individual nucleosomes and at the level of subnuclear organization of chromatin, implying that macroH2A is a multifunctional repressor of chromatin in vivo.

Despite the interest in macroH2A's roles in cell state maintenance and cell fate decisions (Creppe et al., 2012; Pasque et al., 2012; Barrero et al., 2013), surprisingly little is known about how it is inherited through cell division. The landmark study on which most of our current insights are based was performed in 2002 using immunofluorescence techniques (Chadwick and Willard, 2002) mostly focused on the association of macroH2A with the inactive X chromosome. We note that our imaging results do not support their immunofluorescence-based observation of a failure of detection of the macrochromatin body at the inactive X chromosome during mitosis, when the signal from the condensed nuclear chromatin reaches the saturation limit of their microscopy (Chadwick and Willard, 2002). On the other hand, their finding that macroH2A reforms following cell division during the G1 phase of the cell cycle is consistent with our imaging and biochemical results. The major value of the current study is to provide an updated fundamental set of observations about macroH2A heritability through cell division, a necessary foundation if we are to progress to the identification of any chaperone-mediated mechanisms that help to target this histone variant to heterochromatin. The discovery of the targeting mechanisms for regional macroH2A deposition during G1 will represent a significant insight into the epigenetic (transcriptional regulatory) mechanisms of cellular memory occurring on a macrodomain scale, a mechanistically underexplored area of research. We recognize the presence of comparably large domain organization in normal cells and in cells with regulatory perturbations, such as partially methylated domains (Gaidatzis et al., 2014) and lamina-associated domains (Guelen et al., 2008), but we lack insight into how these large domains are coordinately regulated. The influences that maintain or perturb large-scale macroH2A targeting will provide valuable insights into transcriptional regulatory influences conferring epigenetic properties to the cell, acting over hundreds to thousands of kilobases.

Materials and methods

Cell lines and tissue culture

HEK 293T cells were grown at 37°C and 5% CO_2 in DMEM containing 4.5 g/liter of glucose, 10% FBS, and 1% penicillin–streptomycin. HEK 293T cells stably expressing SNAP-H3 or macroH2A1.2 were selected with Zeocin (100 nM) treatment for 3 wk after transfection of linearized vector. HEK 293T stably expressing cell cycle marker was established by lentivirus packaging system as previously described (Naldini et al., 1996). The cells expressing each gene were selected by FACS.

Plasmid construction

To generate the plasmids expressing SNAP-H3 and SNAP-macroH2A, the $pSNAP_f$ vector produced from New England Biolabs was used. Due to the drug incompatibility in HEK 293T cells, we replaced the existing Neomycin selection gene with Zeocin. After creating the $pSNAP_f$-Zeocin vector, the cDNA of H3.1 isolated from a human cDNA library or the cDNA for macroH2A1.2 from pCS2+ macroH2A1.2-GFP-HA (30515; Addgene) was cloned into the $pSNAP_f$-Zeocin vector. The Fucci cell cycle indicator (Sakaue-Sawano et al., 2008), which expresses TagBFP-tagged hCdt1 (30–120) and mCherry-tagged hGeminin (1–110) with a T2A self-cleaving peptide T2A (Thosea asigna virus 2A; Ryan et al., 1991) was cloned into a lentiviral vector. The maps of all constructs are shown in Fig. S1. For the construct expressing mCherry-tagged macroH2A1.2, the results shown in Fig. S1, GFP was replaced by mCherry in pCS2+ macroH2A1.2-GFP-HA (30515; Addgene).

Synchronization of cell cycle, histone labeling using SNAP tagging, and EdU incorporation

Cell synchronization at the G1/S or M phase was performed using double thymidine block or mitotic shake-off methods (Jackman and O'Connor, 2001), optimizing the incubation time and drug concentrations for this study. The cells were synchronized at the G1/S transition using a treatment of 2 mM thymidine for 16 h, releasing from thymidine for 9 h, and treating again with 2 mM thymidine again for 17 h. SNAP-tagged histones were labeled with cell permeable SNAP-substrates, SNAP-Cell Oregon Green (1 μM), SNAP-Cell TMR (1 μM) or blocked with nonfluorescent SNAP-substrates, SNAP-cell Block (10 μM), for 30 min at 37°C in 5% CO_2. Proliferating cells were detected using the Click-iT EdU Cell Proliferation Assay (Life Technologies). To collect mitotic cells, a mitotic shake-off was performed 12 h after treatment with 20 nM Nocodazole following treatment with 2 mM thymidine for 24 h.

Fixed-cell image acquisition

For imaging of fixed cells, cells were grown on poly-L-lysine–coated coverslips, fixed in 4% paraformaldehyde for 15 min at room temperature, and then permeabilized with 0.2% Tween in PBS for 15 min at RT. For the immunofluorescence experiment in Fig. S1, the cells were treated in PBS containing 3% BSA for 1 h and then incubated with primary antibody (1/1,000 dilution) overnight. After washing with PBS three times, the cells were incubated with secondary antibody (1/10,000 dilution) for 30 min. The cells were mounted with Prolong Diamond Antifade Mountant with DAPI. Images were acquired with an Olympus BX61 widefield, epifluorescent microscope using a 60× 1.4 PlanApo objective. Filter sets were used for DAPI (model DAPI-5060C-Zero; Semrock), Cy3 (Chroma model 41007), FITC (model FITC-5050A-Zero; Semrock), and Cy5 (model Cy5-4040C-Zero; Semrock), with an EXFO X-Cite Series 120 PC metal halide light source, Photometrics Cool SNAP HQ CCD camera, Olympus Type-F immersion oil (nd 1.516), and Molecular Devices

Metamorph acquisition software. Cells were optically sectioned using a 0.5-µm Z step, spanning a 10.0-µm Z depth in total. Exposure times of 20–200 ms were typically used to acquire each plane in the Cy3, Cy5, and FITC channels, and ∼12 ms were used to acquire each plane in the DAPI channel.

Live-cell imaging acquisition

For live-cell imaging, we replaced the growth medium with FluoroBrite DMEM Media containing 10% FBS, 1% penicillin/streptomycin, and GlutaMax before imaging. Widefield images of mitotic cells were taken on an IX-81 stand (Olympus). The microscope was equipped as described previously (Wu et al., 2016). The cells were kept at 37°C with a stage top incubator (INUBH-ZILCS-F1; Tokai Hit) in 5% CO_2. Cells were optically sectioned using a 500-nm Z step, spanning a 5.0-µm Z depth in total. 50-ms exposure times were used to acquire each plane in all channels.

Cell cycle–specific native AChE using SNAP-biotin

A total of 1–2 × 10^7 cells were suspended in 1 ml extraction buffer (10 mM Hepes, pH 7.5, 10 mM KCl, 1.5 mM $MgCl_2$, 0.34 M Sucrose, 10% Glycerol, 0.2% NP-40, and protease inhibitor) after treatment with the SNAP-block approach and then lysing the cells for 10 min on ice. Nuclei were pelleted (6,500 rpm, 5 min, 4°C) and the supernatant discarded. Isolated nuclei were washed with 1 ml of extraction buffer without NP-40 and suspended in 0.5 ml digestion buffer (50 mM Tris, pH 7.5, 1 mM $CaCl_2$, 1 mM DTT, 1 mM PMSF, and protease inhibitor). The DNA concentration was detected using 2 M NaCl adjusting the concentration of the chromatin fraction to 1 µg/ml. Newly incorporated macroH2A in 1 ml of nuclei (1 µg/ml) was labeled with SNAP-Biotin (1 µM) at 4°C for 30 min. 10 µl of 50 mU/µl micrococcal nuclease (Sigma) was added and incubated at 37°C for 10 min. The reaction was stopped by supplementing with 100 µl of 0.1 M EGTA. Digested chromatin was centrifuged at 8,000 g at 4°C for 5 min. A sample of this material was used as the source of the input (unenriched) control DNA for the AChE-seq experiments.

The supernatant was labeled as S1 and stored at 4°C, and the pellet was suspended in lysis buffer (Tris, pH 7.4, 0.2 M EDTA, and protease inhibitor) and dialyzed against 2 liters of dialysis buffer (Tris, pH 7.4, and 0.2 mM EDTA) overnight. The chromatin fraction was centrifuged at 500 x*g* for 10 min at 4°C, and the supernatant was combined with the S1 sample, keeping 100 µl of this fraction as our input sample. 50 µl of streptavidin magnet beads preblocked with 1 mg/ml BSA and 0.3 mg/ml salmon sperm DNA was added to 150 µg of the chromatin fraction and rotated for 2 h at 4°C. Beads were washed five times, and DNA isolation was performed followed by a standard ChIP-seq library preparation as we have described previously (Ramos et al., 2015). Input and pull-down samples were sequenced using the Illumina HiSeq 2500 generating 100-bp paired-end reads and analyzed as describe in the following section. Our AChE-seq results were validated using qPCR of the input and pull-down samples (AChE-qPCR), representing the equivalent of ChIP-qPCR, using the Power SYBR Green PCR Master Mix (Thermo Fisher Scientific). As shown in Fig. 5 B, we used a sample treated otherwise identically but without conjugating biotin to the SNAP tag as a negative control for AChE-qPCR. The levels of fold-enrichment were determined from C_T values normalized by negative control. The list of primers is shown in Table S1.

AChE-seq data analysis

Libraries were sequenced using Illumina HiSeq 2500 100-bp paired-end sequencing in our institutional Epigenomics Shared Facility. The sequencing reads were aligned to the hg19 reference genome using *BWA* (version 0.7.10). Alignments were generated in the SAM format and then transformed and sorted into BAM files using *SAMtools* (version 1.2). To remove duplicates and to down-sample all datasets to an equivalent number of reads (127 million), the sorted sequences in BAM format were processed using *Picard-tools* (version 1.119). Down-sampled unique reads were transformed into BED format using *BEDtools2* (version 2.24.0). To identify domains of enrichment from the AChE-seq data, we created genomic windows of 1–1,000 kb using the hg19 reference genome and measured the number of normalized reads for each AChE-seq sample set, including input, using *BEDtools2* (version 2.24.0). The enrichment for each AChE-seq sample set (S–G2 and G1) was calculated by the number of reads in each genomic window normalized by the number of input reads in that window. The distribution of the enrichment ratio for each window was visualized using density plots generated using R. For permutation testing, shuffled sequences (100 iterations) were created with *BEDtools2* (version 2.24.0). The window size with a bimodal pattern of enrichment and the cutoff defining the enriched windows were determined with the *pastecs* library in R. These enriched windows were intersected with CytoBand annotations from the UCSC Genome browser using *BEDtools2* (version 2.24.0). Custom code and parameters used in this project are available at GitHub (https://github.com/hnst/Sato-et-al).

Mononucleosome isolation and immunoprecipitation

Chromatin isolation and MNase digestion were performed as described in the previous section. The salt concentration in the nucleosome fraction was adjusted to be 0.65 M NaCl, applied on the top of a 5–28% sucrose gradient (20 mM Tris, pH 7.5, 150 mM NaCl, and 0.2 mM PMSF) and ultracentrifuged for 15 h at 36,000 rpm at 4°C using a Beckman SW41 rotor. Nucleosomes were fractionated by taking samples sequentially from the top. DNA was purified from an aliquot from each fraction, and mononucleosome fractions were identified by the size of DNA fragments. The purified mononucleosome fraction was incubated with 5 µl of anti-SNAP antibody (New England Biolabs) or rabbit IgG for 2 h at 4°C. 50 µl of protein A/G magnet beads (26162; Thermo Fisher Scientific) preblocked with 1 mg/ml BSA was added and rotated for 1 h at 4°C. The beads were washed three times, and proteins were eluted by SDS loading buffer.

FCS

For FCS analysis, 150 µl of purified nuclei (1 mg/ml) was labeled with 5 nmol of SNAP–Oregon Green for 2 h at RT followed by MNase digestion and ultracentrifugation as described above.

The mononucleosome fraction was measured on 5% BSA-coated 8-well-chambered coverglass (155411; Thermo Fisher Scientific) using a home-built two-photon fluorescence fluctuation microscope described previously (Wu et al., 2015).

Data analysis

Quantifications and statistical analyses in imaging acquisitions and in Western blotting were performed using ImageJ and GraphPad Prism 7. Quantifications and statistical analyses in FACS analyses were performed in FlowJo.

Data and software availability

The AChE-seq data reported in this paper are available from the NCBI Sequence Read Archive under accession no. SRP092259 (https://trace.ncbi.nlm.nih.gov/Traces/sra/sra.cgi?study=SRP092259).The custom code used in this project is available at GitHub (https://github.com/hnst/Sato-et-al).

Online supplemental material

Fig. S1 shows the reagents used in this study. Fig. S2 shows imaging results of immunofluorescence of the inactive X territories in HEK 293T cells using anti-macroH2A and anti-H3K27me3 antibodies, and a time-lapse image of mCherry-labeled macroH2A in a cell undergoing mitosis. Fig. S3 shows the construct design for the Fucci system we used and flow cytometry data allowing us to define the timing of the HEK 293T cell cycle. Fig. S4 shows results of AChE-seq data analysis. Fig. S5 shows fluorescence correlation microscopy and Western blot studies of macroH2A. Video 1 shows live-cell imaging of the images shown in Fig. S2 B. Videos 2 and 3 show the live-cell imaging of the images shown in Fig. 4 A.

Acknowledgments

We thank members of the Greally and Singer laboratories for discussions, Professor Noel Lowndes and Dr. Joseph McCarter (National University of Ireland, Galway) for advice on protocols, the Einstein Epigenomics Shared Facility and FACS and Genomics cores, and Einstein's Center for Epigenomics. We also thank L. Lavis for SNAP-JF646 and Y. Kong for help with AChE-seq analysis.

This work was supported by National Institutes of Health grant R01 DA030317 (to J.M. Greally).

The authors declare no competing financial interests.

Author contributions: Conceptualization, H. Sato and J.M. Greally; methodology, H. Sato, B. Wu, R.H. Singer, and J.M. Greally; formal analysis, H. Sato, B. Wu, and F. Delahaye; investigation, H. Sato; resources, R.H. Singer; data curation, H. Sato; writing of original draft, H. Sato and J.M. Greally; writing—review and editing, H. Sato, R.H. Singer, and J.M. Greally; visualization, H. Sato and J.M. Greally; supervision, R.H. Singer and J.M. Greally; project administration, J.M. Greally; funding acquisition, J.M. Greally.

Submitted: 20 November 2018
Revised: 20 March 2019
Accepted: 19 April 2019

References

Alabert, C., T.K. Barth, N. Reverón-Gómez, S. Sidoli, A. Schmidt, O.N. Jensen, A. Imhof, and A. Groth. 2015. Two distinct modes for propagation of histone PTMs across the cell cycle. *Genes Dev.* 29:585–590. https://doi.org/10.1101/gad.256354.114

Amor, D.J., and K.H.A. Choo. 2002. Neocentromeres: role in human disease, evolution, and centromere study. *Am. J. Hum. Genet.* 71:695–714. https://doi.org/10.1086/342730

Angelov, D., A. Molla, P.-Y. Perche, F. Hans, J. Côté, S. Khochbin, P. Bouvet, and S. Dimitrov. 2003. The histone variant macroH2A interferes with transcription factor binding and SWI/SNF nucleosome remodeling. *Mol. Cell.* 11:1033–1041. https://doi.org/10.1016/S1097-2765(03)00100-X

Augui, S., E.P. Nora, and E. Heard. 2011. Regulation of X-chromosome inactivation by the X-inactivation centre. *Nat. Rev. Genet.* 12:429–442. https://doi.org/10.1038/nrg2987

Bailey, T., P. Krajewski, I. Ladunga, C. Lefebvre, Q. Li, T. Liu, P. Madrigal, C. Taslim, and J. Zhang. 2013. Practical guidelines for the comprehensive analysis of ChIP-seq data. *PLOS Comput. Biol.* 9:e1003326. https://doi.org/10.1371/journal.pcbi.1003326

Barrero, M.J., B. Sese, M. Martí, and J.C. Izpisua Belmonte. 2013. Macro histone variants are critical for the differentiation of human pluripotent cells. *J. Biol. Chem.* 288:16110–16116. https://doi.org/10.1074/jbc.M113.466144

Bergmann, J.H., M.G. Rodríguez, N.M.C. Martins, H. Kimura, D.A. Kelly, H. Masumoto, V. Larionov, L.E.T. Jansen, and W.C. Earnshaw. 2011. Epigenetic engineering shows H3K4me2 is required for HJURP targeting and CENP-A assembly on a synthetic human kinetochore. *EMBO J.* 30:328–340. https://doi.org/10.1038/emboj.2010.329

Borghesan, M., C. Fusilli, F. Rappa, C. Panebianco, G. Rizzo, J.A. Oben, G. Mazzoccoli, C. Faulkes, I. Pata, A. Agodi, et al. 2016. DNA Hypomethylation and Histone Variant macroH2A1 Synergistically Attenuate Chemotherapy-Induced Senescence to Promote Hepatocellular Carcinoma Progression. *Cancer Res.* 76:594–606. https://doi.org/10.1158/0008-5472.CAN-15-1336

Bostick, M., J.K. Kim, P.-O. Estève, A. Clark, S. Pradhan, and S.E. Jacobsen. 2007. UHRF1 plays a role in maintaining DNA methylation in mammalian cells. *Science.* 317:1760–1764. https://doi.org/10.1126/science.1147939

Boyarchuk, E., D. Filipescu, I. Vassias, S. Cantaloube, and G. Almouzni. 2014. The histone variant composition of centromeres is controlled by the pericentric heterochromatin state during the cell cycle. *J. Cell Sci.* 127:3347–3359. https://doi.org/10.1242/jcs.148189

Chadwick, B.P., and H.F. Willard. 2002. Cell cycle-dependent localization of macroH2A in chromatin of the inactive X chromosome. *J. Cell Biol.* 157:1113–1123. https://doi.org/10.1083/jcb.200112074

Chakravarthy, S., and K. Luger. 2006. The histone variant macro-H2A preferentially forms "hybrid nucleosomes". *J. Biol. Chem.* 281:25522–25531. https://doi.org/10.1074/jbc.M602258200

Chen, Y., and J.D. Müller. 2007. Determining the stoichiometry of protein heterocomplexes in living cells with fluorescence fluctuation spectroscopy. *Proc. Natl. Acad. Sci. USA.* 104:3147–3152. https://doi.org/10.1073/pnas.0606557104

Cleveland, D.W., Y. Mao, and K.F. Sullivan. 2003. Centromeres and kinetochores: from epigenetics to mitotic checkpoint signaling. *Cell.* 112:407–421. https://doi.org/10.1016/S0092-8674(03)00115-6

Coleman, R.T., and G. Struhl. 2017. Causal role for inheritance of H3K27me3 in maintaining the OFF state of a *Drosophila* HOX gene. *Science.* 356:eaai8236. https://doi.org/10.1126/science.aai8236

Costanzi, C., and J.R. Pehrson. 1998. Histone macroH2A1 is co ncentrated in the inactive X chromosome of female mammals. *Nature.* 393:599–601. https://doi.org/10.1038/31275

Creppe, C., P. Janich, N. Cantariño, M. Noguera, V. Valero, E. Musulén, J. Douet, M. Posavec, J. Martín-Caballero, L. Sumoy, et al. 2012. MacroH2A1 regulates the balance between self-renewal and differentiation commitment in embryonic and adult stem cells. *Mol. Cell. Biol.* 32:1442–1452. https://doi.org/10.1128/MCB.06323-11

Csankovszki, G., B. Panning, B. Bates, J.R. Pehrson, and R. Jaenisch. 1999. Conditional deletion of Xist disrupts histone macroH2A localization but not maintenance of X inactivation. *Nat. Genet.* 22:323–324. https://doi.org/10.1038/11887

Douet, J., D. Corujo, R. Malinverni, J. Renauld, V. Sansoni, M. Posavec Marjanović, N. Cantariño, V. Valero, F. Mongelard, P. Bouvet, et al. 2017. MacroH2A histone variants maintain nuclear organization and heterochromatin architecture. *J. Cell Sci.* 130:1570–1582. https://doi.org/10.1242/jcs.199216

Dunleavy, E.M., G. Almouzni, and G.H. Karpen. 2011. H3.3 is deposited at centromeres in S phase as a placeholder for newly assembled CENP-A in G_1 phase. *Nucleus.* 2:146–157. https://doi.org/10.4161/nucl.2.2.15211

Ferguson-Smith, A.C. 2011. Genomic imprinting: the emergence of an epigenetic paradigm. *Nat. Rev. Genet.* 12:565–575. https://doi.org/10.1038/nrg3032

French, B.T., and A.F. Straight. 2013. Swapping CENP-A at the centromere. *Nat. Cell Biol.* 15:1028–1030. https://doi.org/10.1038/ncb2833

Gaidatzis, D., L. Burger, R. Murr, A. Lerch, S. Dessus-Babus, D. Schübeler, and M.B. Stadler. 2014. DNA sequence explains seemingly disordered methylation levels in partially methylated domains of Mammalian genomes. *PLoS Genet.* 10:e1004143. https://doi.org/10.1371/journal.pgen.1004143

Gamble, M.J., K.M. Frizzell, C. Yang, R. Krishnakumar, and W.L. Kraus. 2010. The histone variant macroH2A1 marks repressed autosomal chromatin, but protects a subset of its target genes from silencing. *Genes Dev.* 24:21–32. https://doi.org/10.1101/gad.1876110

Gautier, A., A. Juillerat, C. Heinis, I.R. Corrêa Jr., M. Kindermann, F. Beaufils, and K. Johnsson. 2008. An engineered protein tag for multiprotein labeling in living cells. *Chem. Biol.* 15:128–136. https://doi.org/10.1016/j.chembiol.2008.01.007

Gaydos, L.J., W. Wang, and S. Strome. 2014. Gene repression. H3K27me and PRC2 transmit a memory of repression across generations and during development. *Science.* 345:1515–1518. https://doi.org/10.1126/science.1255023

Ginno, P.A., L. Burger, J. Seebacher, V. Iesmantavicius, and D. Schübeler. 2018. Cell cycle-resolved chromatin proteomics reveals the extent of mitotic preservation of the genomic regulatory landscape. *Nat. Commun.* 9:4048. https://doi.org/10.1038/s41467-018-06007-5

Goldberg, A.D., L.A. Banaszynski, K.-M. Noh, P.W. Lewis, S.J. Elsaesser, S. Stadler, S. Dewell, M. Law, X. Guo, X. Li, et al. 2010. Distinct factors control histone variant H3.3 localization at specific genomic regions. *Cell.* 140:678–691. https://doi.org/10.1016/j.cell.2010.01.003

Guelen, L., L. Pagie, E. Brasset, W. Meuleman, M.B. Faza, W. Talhout, B.H. Eussen, A. de Klein, L. Wessels, W. de Laat, and B. van Steensel. 2008. Domain organization of human chromosomes revealed by mapping of nuclear lamina interactions. *Nature.* 453:948–951. https://doi.org/10.1038/nature06947

Gurard-Levin, Z.A., J.-P. Quivy, and G. Almouzni. 2014. Histone chaperones: assisting histone traffic and nucleosome dynamics. *Annu. Rev. Biochem.* 83:487–517. https://doi.org/10.1146/annurev-biochem-060713-035536

Hansen, K.H., A.P. Bracken, D. Pasini, N. Dietrich, S.S. Gehani, A. Monrad, J. Rappsilber, M. Lerdrup, and K. Helin. 2008. A model for transmission of the H3K27me3 epigenetic mark. *Nat. Cell Biol.* 10:1291–1300. https://doi.org/10.1038/ncb1787

Henikoff, S., and J.M. Greally. 2016. Epigenetics, cellular memory and gene regulation. *Curr. Biol.* 26:R644–R648. https://doi.org/10.1016/j.cub.2016.06.011

Hernández-Muñoz, I., A.H. Lund, P. van der Stoop, E. Boutsma, I. Muijrers, E. Verhoeven, D.A. Nusinow, B. Panning, Y. Marahrens, and M. van Lohuizen. 2005. Stable X chromosome inactivation involves the PRC1 Polycomb complex and requires histone MACROH2A1 and the CULLIN3/SPOP ubiquitin E3 ligase. *Proc. Natl. Acad. Sci. USA.* 102:7635–7640. https://doi.org/10.1073/pnas.0408918102

Jackman, J., and P.M. O'Connor. 2001. Methods for synchronizing cells at specific stages of the cell cycle. *Curr. Protoc. Cell Biol.* Chapter 8:Unit 8.3.

Jansen, L.E.T., B.E. Black, D.R. Foltz, and D.W. Cleveland. 2007. Propagation of centromeric chromatin requires exit from mitosis. *J. Cell Biol.* 176:795–805. https://doi.org/10.1083/jcb.200701066

Kizer, K.O., H.P. Phatnani, Y. Shibata, H. Hall, A.L. Greenleaf, and B.D. Strahl. 2005. A novel domain in Set2 mediates RNA polymerase II interaction and couples histone H3 K36 methylation with transcript elongation. *Mol. Cell. Biol.* 25:3305–3316. https://doi.org/10.1128/MCB.25.8.3305-3316.2005

Koren, A., and S.A. McCarroll. 2014. Random replication of the inactive X chromosome. *Genome Res.* 24:64–69. https://doi.org/10.1101/gr.161828.113

Lappalainen, T., and J.M. Greally. 2017. Associating cellular epigenetic models with human phenotypes. *Nat. Rev. Genet.* 18:441–451. https://doi.org/10.1038/nrg.2017.32

Laprell, F., K. Finkl, and J. Müller. 2017. Propagation of Polycomb-repressed chromatin requires sequence-specific recruitment to DNA. *Science.* 356:85–88. https://doi.org/10.1126/science.aai8266

Le Thomas, A., A.K. Rogers, A. Webster, G.K. Marinov, S.E. Liao, E.M. Perkins, J.K. Hur, A.A. Aravin, and K.F. Tóth. 2013. Piwi induces piRNA-guided transcriptional silencing and establishment of a repressive chromatin state. *Genes Dev.* 27:390–399. https://doi.org/10.1101/gad.209841.112

Mehrotra, P.V., D. Ahel, D.P. Ryan, R. Weston, N. Wiechens, R. Kraehenbuehl, T. Owen-Hughes, and I. Ahel. 2011. DNA repair factor APLF is a histone chaperone. *Mol. Cell.* 41:46–55. https://doi.org/10.1016/j.molcel.2010.12.008

Müller, S., and G. Almouzni. 2014. A network of players in H3 histone variant deposition and maintenance at centromeres. *Biochim. Biophys. Acta.* 1839:241–250. https://doi.org/10.1016/j.bbagrm.2013.11.008

Naldini, L., U. Blömer, P. Gallay, D. Ory, R. Mulligan, F.H. Gage, I.M. Verma, and D. Trono. 1996. In vivo gene delivery and stable transduction of nondividing cells by a lentiviral vector. *Science.* 272:263–267. https://doi.org/10.1126/science.272.5259.263

Ng, K., N. Daigle, A. Bancaud, T. Ohhata, P. Humphreys, R. Walker, J. Ellenberg, and A. Wutz. 2011. A system for imaging the regulatory noncoding Xist RNA in living mouse embryonic stem cells. *Mol. Biol. Cell.* 22:2634–2645. https://doi.org/10.1091/mbc.e11-02-0146

Pasque, V., A. Radzisheuskaya, A. Gillich, R.P. Halley-Stott, M. Panamarova, M. Zernicka-Goetz, M.A. Surani, and J.C.R. Silva. 2012. Histone variant macroH2A marks embryonic differentiation in vivo and acts as an epigenetic barrier to induced pluripotency. *J. Cell Sci.* 125:6094–6104. https://doi.org/10.1242/jcs.113019

Pehrson, J.R., and V.A. Fried. 1992. MacroH2A, a core histone containing a large nonhistone region. *Science.* 257:1398–1400. https://doi.org/10.1126/science.1529340

Petryk, N., M. Dalby, A. Wenger, C.B. Stromme, A. Strandsby, R. Andersson, and A. Groth. 2018. MCM2 promotes symmetric inheritance of modified histones during DNA replication. *Science.* 361:1389–1392. https://doi.org/10.1126/science.aau0294

Quénet, D., and Y. Dalal. 2014. A long non-coding RNA is required for targeting centromeric protein A to the human centromere. *eLife.* 3:e03254. https://doi.org/10.7554/eLife.03254

Ramos, M.-P., N.A. Wijetunga, A.S. McLellan, M. Suzuki, and J.M. Greally. 2015. DNA demethylation by 5-aza-2′-deoxycytidine is imprinted, targeted to euchromatin, and has limited transcriptional consequences. *Epigenetics Chromatin.* 8:11. https://doi.org/10.1186/s13072-015-0004-x

Ratnakumar, K., L.F. Duarte, G. LeRoy, D. Hasson, D. Smeets, C. Vardabasso, C. Bönisch, T. Zeng, B. Xiang, D.Y. Zhang, et al. 2012. ATRX-mediated chromatin association of histone variant macroH2A1 regulates α-globin expression. *Genes Dev.* 26:433–438. https://doi.org/10.1101/gad.179416.111

Reverón-Gómez, N., C. González-Aguilera, K.R. Stewart-Morgan, N. Petryk, V. Flury, S. Graziano, J.V. Johansen, J.S. Jakobsen, C. Alabert, and A. Groth. 2018. Accurate Recycling of Parental Histones Reproduces the Histone Modification Landscape during DNA Replication. *Mol. Cell.* 72:239–249.e5. https://doi.org/10.1016/j.molcel.2018.08.010

Ryan, M.D., A.M. King, and G.P. Thomas. 1991. Cleavage of foot-and-mouth disease virus polyprotein is mediated by residues located within a 19 amino acid sequence. *J. Gen. Virol.* 72:2727–2732. https://doi.org/10.1099/0022-1317-72-11-2727

Sakaue-Sawano, A., H. Kurokawa, T. Morimura, A. Hanyu, H. Hama, H. Osawa, S. Kashiwagi, K. Fukami, T. Miyata, H. Miyoshi, et al. 2008. Visualizing spatiotemporal dynamics of multicellular cell-cycle progression. *Cell.* 132:487–498. https://doi.org/10.1016/j.cell.2007.12.033

Sharif, J., M. Muto, S. Takebayashi, I. Suetake, A. Iwamatsu, T.A. Endo, J. Shinga, Y. Mizutani-Koseki, T. Toyoda, K. Okamura, et al. 2007. The SRA protein Np95 mediates epigenetic inheritance by recruiting Dnmt1 to methylated DNA. *Nature.* 450:908–912. https://doi.org/10.1038/nature06397

Suzuki, M., M. Oda, M.-P. Ramos, M. Pascual, K. Lau, E. Stasiek, F. Agyiri, R.F. Thompson, J.L. Glass, Q. Jing, et al. 2011. Late-replicating heterochromatin is characterized by decreased cytosine methylation in the human genome. *Genome Res.* 21:1833–1840. https://doi.org/10.1101/gr.116509.110

Tanasijevic, B., and T.P. Rasmussen. 2011. X chromosome inactivation and differentiation occur readily in ES cells doubly-deficient for macroH2A1 and macroH2A2. *PLoS One.* 6:e21512. https://doi.org/10.1371/journal.pone.0021512

Van Hooser, A., D.W. Goodrich, C.D. Allis, B.R. Brinkley, and M.A. Mancini. 1998. Histone H3 phosphorylation is required for the initiation, but not maintenance, of mammalian chromosome condensation. *J. Cell Sci.* 111:3497–3506.

Wang, J., X. Liu, Z. Dou, L. Chen, H. Jiang, C. Fu, G. Fu, D. Liu, J. Zhang, T. Zhu, et al. 2014. Mitotic regulator Mis18β interacts with and specifies the

centromeric assembly of molecular chaperone holliday junction recognition protein (HJURP). *J. Biol. Chem.* 289:8326–8336. https://doi.org/10.1074/jbc.M113.529958

Wu, B., V. Miskolci, H. Sato, E. Tutucci, C.A. Kenworthy, S.K. Donnelly, Y.J. Yoon, D. Cox, R.H. Singer, and L. Hodgson. 2015. Synonymous modification results in high-fidelity gene expression of repetitive protein and nucleotide sequences. *Genes Dev.* 29:876–886. https://doi.org/10.1101/gad.259358.115

Wu, B., C. Eliscovich, Y.J. Yoon, and R.H. Singer. 2016. Translation dynamics of single mRNAs in live cells and neurons. *Science.* 352:1430–1435. https://doi.org/10.1126/science.aaf1084

Xu, M., C. Long, X. Chen, C. Huang, S. Chen, and B. Zhu. 2010. Partitioning of histone H3-H4 tetramers during DNA replication-dependent chromatin assembly. *Science.* 328:94–98. https://doi.org/10.1126/science.1178994

Yildirim, O., J.-H. Hung, R.J. Cedeno, Z. Weng, C.J. Lengner, and O.J. Rando. 2014. A system for genome-wide histone variant dynamics in ES cells reveals dynamic MacroH2A2 replacement at promoters. *PLoS Genet.* 10: e1004515. https://doi.org/10.1371/journal.pgen.1004515

Yu, C., H. Gan, A. Serra-Cardona, L. Zhang, S. Gan, S. Sharma, E. Johansson, A. Chabes, R.-M. Xu, and Z. Zhang. 2018. A mechanism for preventing asymmetric histone segregation onto replicating DNA strands. *Science.* 361:1386–1389. https://doi.org/10.1126/science.aat8849